Available online at www.sciencedirect.com

ScienceDirect

journal homepage: www.elsevier.com/locate/he

Environmental analysis and optimization of fuel cells integrated with organic rankine cycle using zeotropic mixture

Tao Hai [a,b,c,*], Masood Ashraf Ali [d,**], As'ad Alizadeh [e,***], Sattam Fahad Almojil [f,****], Aman Sharma [g], Abdulaziz Ibrahim Almohana [f], Abdulrhman Fahmi Alali [f]

[a] School of Computer and Information, Qiannan Normal University for Nationalities, Duyun, Guizhou, 558000, China
[b] Key Laboratory of Advanced Manufacturing Technology of the Ministry of Education, Guizhou University, Guizhou, 550025, China
[c] Institute for Big Data Analytics and Artificial Intelligence (IBDAAI), Universiti Teknologi MARA, 40450 Shah Alam, Selangor, Malaysia
[d] Department of Industrial Engineering, College of Engineering, Prince Sattam Bin Abdulaziz University, Alkharj 16273, Saudi Arabia
[e] Department of Civil Engineering, College of Engineering, Cihan University-Erbil, Erbil, Iraq
[f] Department of Civil Engineering, College of Engineering, King Saud University, P.O. Box 800, Riyadh 11421, Saudi Arabia
[g] Institute of Engineering and Technology, GLA University, Mathura, UP 281406, India

HIGHLIGHTS

- A hybrid electricity generation system including PEM FC and ORC is analyzed.
- Exergy Efficiency and economic analysis are considered for system evaluation.
- Three novel zeotropic mixtures are examined as the working fluid of the ORC system.
- A Parametric Study and optimization are conducted in this research paper.

ARTICLE INFO

Article history:
Received 21 November 2022
Received in revised form
13 January 2023
Accepted 27 January 2023
Available online 23 February 2023

Keywords:
Fuel cell
Organic rankine cycle
Zeotropic mixture

* Corresponding author.
** Corresponding author.
*** Corresponding author.
**** Corresponding author.
E-mail addresses: haitao@bjwlxy.edu.cn (T. Hai), mas.ali@psau.edu.sa (M. Ashraf Ali), asad.alizadeh2010@gmail.com (A. Alizadeh), salmojil@ksu.edu.sa (S. Fahad Almojil).

https://doi.org/10.1016/j.ijhydene.2023.01.340

ABSTRACT

The use of fuel cell (FC) is considered one of the methods of producing electricity with relatively high efficiency. So, it has attracted many researchers' attention to develop and improve its performance. The present study deals with the technical-economic optimal design of a hybrid power generation system based on a Proton Exchange Membrane (PEM) FC combined with an Organic Rankine Cycle (ORC). ORC is used to recover the generated heat in PEM FC. The decision variables of this study include FC operating pressure and temperature, current density, FC area, the quantity of FC, and operating parameters of the ORC system, including HRVG PPTD, condenser PPTD, and refrigerant mass fraction in zeotropic mixture. In this study, three zeotropic mixtures, including R11-R245fa, R11-R123, and R123-R245fa, are studied as the working fluid of the ORC system. The objective functions considered to be optimized are the system's exergy efficiency and total cost rate

Environmental Analysis
Multi-objective optimization
Fuel cell degradation

(TCR). Finally, it is observed that the highest exergy efficiency is obtained using the zeotropic mixture R11-R245fa with a value of 54.15%, and the lowest TCR is obtained with the mixture R11-R123 with a value of 0.65 $/s. Zeotropic mixture R11-R123 has the exergoenvironmental index, environmental damage effectiveness index, and exergy stability factor of 0.5506, 1.277, and 0.4750, respectively.

Introduction

Due to the rising apprehensions about the ever-increasing reduction of fossil fuels and environmental pollution, attention has been paid to alternative solutions for using clean energy in the past decades. A FC is a device for energy conversion which converts the fuel chemical energy into electricity, heat, and water without a combustion process. Therefore, it leads to the reduction of environmental pollution [32]. Also, since the conversion of fuel chemical energy into power is not done through heat transfer, its energy conversion efficiency is not limited to the efficiency of the Carnot cycle [1,33,34]. Among the different kinds of FCs, the PEM is one of the most appropriate types because it can be used in both portable and stationary applications. Also, the PEM FC has such features as low operating temperature, fast start-up, fast response time, and the ability to produce a wide range of power [2].

In general, the electrochemical reaction that occurs in a PEM FC is simple. On the anode of the FC, hydrogens are breakdown into H^+ and free electrons. Free electrons are moved from the anode to the cathode through the external circuit. Also, the hydrogen ions inside the electrolyte are sent from the anode to the cathode. At the cathode electrode, electrons and H^+ combine with O_2, resulting in water and heat generation. A PEM FC has about 50–60% energy conversion efficiency. Therefore, PEM FC generates the same amount of heat and electricity. In a FC, a cooling system is needed to eliminate the generated heat and maintain the temperature uniformity inside it [35,36].

In recent years, several types of research have been conducted on developing PEM FCs. Also, finding an efficient way to recover the generated heat in the PEM FC system is one of the topics investigated. Several studies have investigated the challenge of recovering generated heat in the PEM FC system. Brigugli et al. [3] investigated the heat recovery from a PEM FC system with a nominal power generation of 5 kW by applying a heat exchanger which absorbs the generated heat of the cathode. The efficiency of the proposed CHP system improved to 85%. Similar analyzes by Aki et al. [4] were considered in the power generation system for residential applications. Nguyen et al. [5] studied a CHP system for distributed energy generation based on PEM FC. Placca et al. [6] proposed a new fuel reforming system using waste heat recovery from a PEM FC system. The results showed that the efficiency of the power plant can increase by more than 20%. Sevjidsuren et al. [7] in 2012 analyzed the exergy of a PEM FC system. They found the optimum value of the air stoichiometric ratio and the operating temperature from the exergy efficiency point of view. In 2003, Grujicic and Chittajallu [8] studied a PEM FC system's optimal design using a two-dimensional single-phase electrochemical model. Kazim in 2003 [9] analyzed the exergy of a PEM FC system with a power of 10 kW. The analysis parameters included operating temperature and pressure, FC voltage, and air stoichiometric ratio. The result of this study showed that the stoichiometric ratio of air should be less than 4 to maintain the relative humidity in the product air and also prevent the dryness of the membrane at high temperatures. Salva et al. [10] 2016 designed a PEM FC to achieve the highest output power for different current density values. In this study, design temperature and pressure, relative humidity of reactants, and cathode stoichiometry are investigated as design variables. Hwang et al. [11]. Proposed a CHP system including a PEM FC for electricity generation. Also, the generated heat is absorbed to warm up water for heating applications. They could receive an efficiency of 81% in CHP mode. In 2019, Li et al. [12] investigated a hybrid power generation system based on geothermal energy. In this study, geothermal energy is used as the heat source of a Rankine flash cycle. Also, a fuel cell is used to generate power, and the thermal energy released by it is recovered for use in the flash Rankine cycle. In 2021, Azad et al. [13] investigated a hybrid power generation system based on PEM FC. The thermal energy released by this system is absorbed by the two-pressure ORC system and used to generate power. Also, a part of the thermal energy released in the condenser is converted into electricity by the thermoelectric generator system. In this study, the effect of using three different zeotropic mixtures is investigated. In 2012, Li [14] investigated the cooling capacity and cooling loop of a PEMFC. The cooling capacity has a direct effect on the operating temperature and thus on the efficiency and generated electricity. It is observed the increase in current density leads to an increase in exergy destruction and a decrease in exergy efficiency. In 2015, Ye et al. [15] investigated two different high-operating-temperature PEMFCs. In the first one, hydrogen entered the fuel cell, and in the second FC, methane gas entered the fuel cell and was converted into hydrogen through reforming. It is observed in both systems, the efficiency and electricity production increases with the increase in operating temperature. In 2016, Gimba et al. [16] modeled a PEMFC. They observed that efficiency increases with increasing operating pressure. Also, they observed the pressure difference between the anode and cathode leads to improved efficiency. In 2011, Barelli et al. [17] investigated a CHP system including PEMFC. They observed that increasing the operating temperature and pressure of the PEMFC leads to an improvement in the efficiency of the CHP system.

Currently, all PEM FCs operate in the temperature range of 50–100 °C. According to the heat source's temperature range, Organic Rankine Cycle (ORC) has the best performance among

all methods for waste heat recovery. Connecting ORC to PEM FC is a practical solution to improve energy conversion efficiency [37]. The present study discusses the thermoeconomic optimal design of a hybrid power generation system based on a PEM FC. The ORC is applied to recover its generated heat and produces extra power. In order to simulate the performance of the studied system, as well as the optimal design of the system a calculation code is developed in MATLAB software. Also, to calculate thermodynamic properties, REFPROP software is linked with MATLAB software [38,39].

For maximum heat recovery, zeotropic mixtures are used as the working fluid of the ORC. When pure fluids are used as working fluid, the evaporation process is performed at constant pressure and temperature, and only the quality of steam increases. However, when zeotropic mixtures are used, the evaporation process is performed at constant pressure with an increase in temperature. Accordingly, the temperature between the hot and the cold fluid in the evaporator decreases, and as a result, exergy destruction in the evaporation process decreases. Therefore, it leads to an improvement in exergy efficiency and net power production [32].

System description

Fig. 1 illustrates the process flow diagram of the studied system. In the studied system, the ORC system is applied as the bottoming cycle of the PEM FC to recover its waste heat. The intended system consists of an air compressor, hydrogen fuel storage source, pressure regulator valve, humidity increase system, FC, ORC system expander, condenser, pump, and protection and control equipment. The required air is compressed by the compressor to the operating pressure of the FC and then enters the cathode. On the other hand, the hydrogen stored in the high-pressure storage tank must have a pressure drop to the working pressure of the FC, which is done by the pressure regulator valve considered in the fuel line. Then the hydrogen enters the anode part of the FC. According to the electrochemical reaction carried out in the FC, DC electric current is produced. After the chemical reaction in the FC, the hydrogen that did not participate in the chemical reaction returns to the fuel supply line. In the ORC system, the generated heat through the FC electrochemical reaction is absorbed in the HRVG by the cycle working fluid. It is converted from a saturated liquid state at the pump's output to superheated steam at the output of the HRVG. After entering the expander and generating mechanical power, it enters the condenser, and after condensation, it is collected in the condensate receiver tank and pressurized up to HRVG pressure, again.

Energy analysis

Proton Exchange Membrane fuel cell

The chemical reactions carried out in the FC with the presence of hydrogen and air as reactants lead to the production of electricity, water, and heat are as follows [40]:

$$\text{Anode}: H_2 \rightarrow 2H^+ + 2e^- \quad (1)$$

$$\text{Cathode}: 2H^+ + 2e^- + \frac{1}{2}O_2 \rightarrow H_2O \quad (2)$$

$$\text{Overall}: H_2 + \frac{1}{2}O_2 \rightarrow H_2O + \text{heat} + \text{electricity} \quad (3)$$

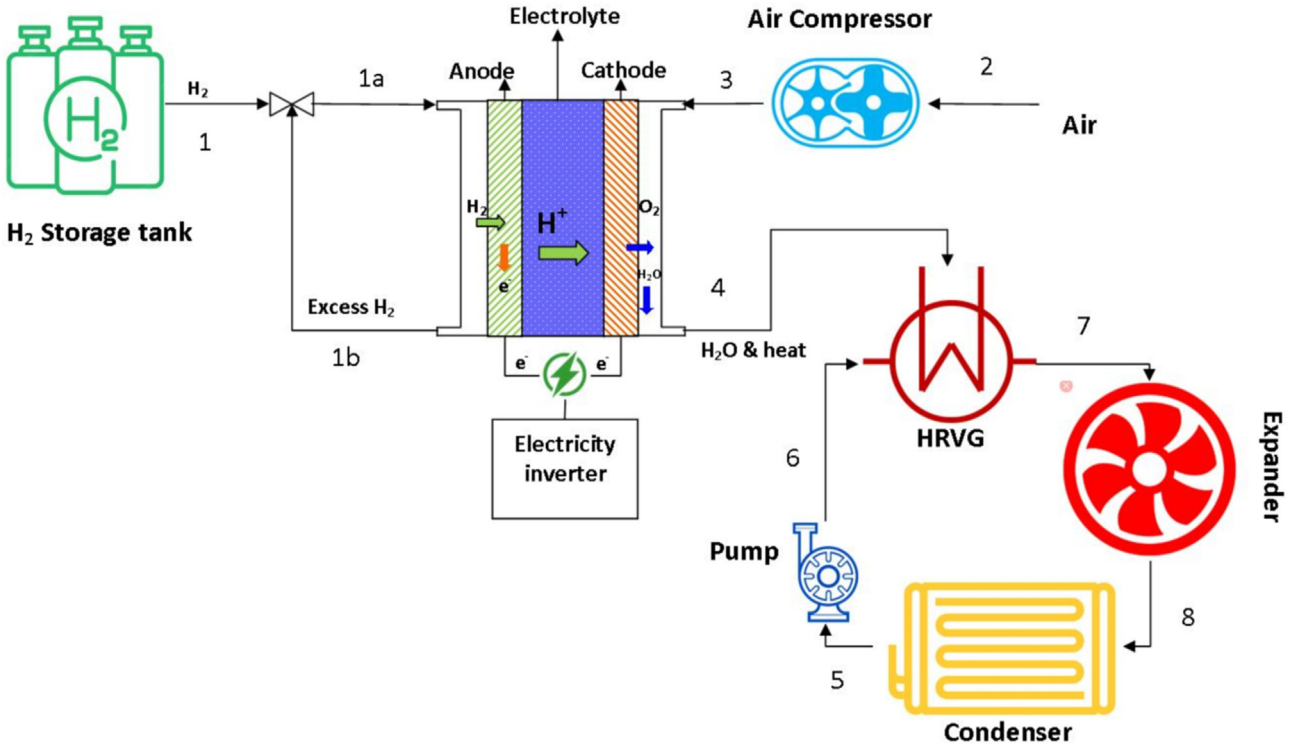

Fig. 1 – Schematic of the considered system.

The maximum voltage which can be achieved from the reversible chemical reaction of the hydrogen and oxygen can be estimated by the Nernst equation as follows [18]:

$$E_{Nernst} = \frac{-\Delta G^0}{n_e F} + \frac{RT_{fc}}{n_e F} \ln\left(\frac{P_{H_2}\sqrt{P_{O_2}}}{P^{sat}_{H_2O}}\right) \quad (4)$$

In Eq. (4), ΔG^0 is the difference of Gibbs free energy, which can be calculated from the following equation according to the enthalpy and entropy changes of the products and reactants of the overall chemical reaction:

$$\Delta G = \Delta H - T\Delta S \quad (5)$$

Also, in Eq. (4), P_{H_2}, P_{O_2}, and $P^{sat}_{H_2O}$ are the partial pressure of the Hydrogen, Oxygen, and water, respectively. According to the water vapor pressure in the anode and cathode, the partial pressure of reactants (H_2 and O_2) can be calculated. For this purpose, the water saturation pressure should be calculated with the following relation [9]:

$$\log_{10}\left(P^{sat}_{H_2O}\right) = -2.1794 + 0.02953t - 9.1837\times10^{-5}t^2 + 1.4454\times10^{-7}t^3 \quad (6)$$

The H_2 and O_2 partial pressure in the anode is given by:

$$P_{H_2} = \left(0.5P^{sat}_{H_2O}\right)\left[\frac{1}{\exp\left(\frac{1.653i}{T_{FC}^{1.334}}\right)} - 1\right] \quad (7)$$

$$P_{O_2} = P\left[1 - x^{sat}_{H_2O} - x^{channel}_{N_2}\exp\left(\frac{0.291i}{T_{FC}^{0.832}}\right)\right] \quad (8)$$

where the molar fractions of the substances are unknown. The molar ratio of water is calculated based on partial pressure, and the molar ratio of nitrogen is calculated based on the stoichiometric ratio of nitrogen in the air entering the FC.

$$x^{sat}_{H_2O} = \frac{P^{sat}_{H_2O}}{P} \quad (9)$$

The molar ratio of nitrogen in the chemical reaction is determined from the logarithmic average of nitrogen input and output of the humidifier with the help of the following relations:

$$x^{channel}_{N_2} = \frac{\left(x^{in}_{N_2} - x^{out}_{N_2}\right)}{\ln\left(\frac{x^{in}_{N_2}}{x^{out}_{N_2}}\right)} \quad (10)$$

$$x^{in}_{N_2} = 0.79\left(1 - x^{sat}_{H_2O}\right) \quad (11)$$

$$x^{out}_{N_2} = \frac{\left(1 - x^{sat}_{H_2O}\right)}{1 + \left(\frac{\lambda_{air}-1}{\lambda_{air}}\right)\left(\frac{0.21}{0.79}\right)} \quad (12)$$

Eq. (4) calculates the maximum voltage. In actual conditions, the FC output voltage is lower than the maximum voltage obtained by the Nernst equation. Three main phenomena lead to voltage decay: voltage decay caused by reaction activation, ohmic voltage decay, and voltage decay due to changes in the reactants and products' concentration [41,42]. By quantifying the mechanisms that cause voltage decay in the FC, the actual voltage of the FC can be calculated.

The voltage decay caused by the reaction activation can be described as [19]:

$$V_{act} = 0.948 - \xi T_{FC} - 0.000076T_{FC}\ln\left(C_{O_2,conc}\right) + 0.000193T_{FC}\ln(I) \quad (13)$$

$$\xi = 0.00286 + 0.0002\ln(A_{cell}) + 0.000043\ln\left(C_{H_2,conc}\right) \quad (14)$$

Where the H_2 and O_2 concentration on the membrane can be written as:

$$C_{O_2,conc} = 1.97\times10^{-7}P_{O_2}\exp\left(\frac{498}{T_{FC}}\right) \quad (15)$$

$$C_{H_2,conc} = 9.174\times10^{-7}P_{H_2}\exp\left(\frac{-77}{T_{FC}}\right) \quad (16)$$

Ohm's law is used to estimate the ohmic voltage decay in all components inside the FC [20]:

$$V_{ohm} = IR_{int} \quad (17)$$

where R_{int} describes all internal current resistances, which will be calculated from the following formula:

$$R_{int} = \frac{r_{mem}L}{A_{cell}} \quad (18)$$

$$r_{mem} = \frac{181.16\left[1 + 0.03i + 0.062\left(\frac{T_{FC}}{303}\right)^2 i^{2.5}\right]}{[\zeta - 0.634 - 3i]exp\left[4.18\left(T_{fc} - \frac{303}{T_{FC}}\right)\right]} \quad (19)$$

where the ζ in Eq. (19) is the water amount on the membrane. In this study, the value of 6 is considered for which. To calculate the voltage decay caused by the change in the concentration of substances in the reactants and products, the following equation is used [19]:

$$V_{conc} = \frac{RT_{fc}}{n_e F}\ln\left(\frac{i_L}{i_L - i}\right) \quad (20)$$

In this study, the maximum intensity of the output current is considered equal to $i_L = 1.5$ A. Finally, the voltage of the FC can be calculated by taking into account the mentioned losses:

$$V_{FC} = E_{Nernst} - V_{act} - V_{ohm} - V_{conc} \quad (21)$$

The following equation provides the output power of the FC system:

$$W_{FC} = N_{cell}V_{FC}I \quad (22)$$

Which W_{FC} is the power obtained from the above relationship for all fuel cells.

Organic rankine cycle

For thermal modeling of the ORC, the relationship of the first law of thermodynamics is presented for all components [21,43]:

Pump power consumption can be calculated as follows:

$$\dot{W}_{PMP} = \dot{m}_{wf}(h_{6s} - h_5) / \eta_{PMP} \quad (23)$$

In the above equation, η_{PMP} is the pump efficiency according to the isentropic concept and is assumed to be 80% in this study.

The rate of recovered heat from FC in HRVG can be calculated as:

$$\dot{Q}_{HRVG} = \dot{m}_{wf}(h_7 - h_{6,ac}) \quad (24)$$

The work produced by the expander is presented as follows:

$$\dot{W}_{EXP} = \dot{m}_{wf}(h_7 - h_8)\eta_{EXP} \quad (25)$$

In the above relationship, η_{EXP} is the expander isentropic efficiency and considered 80% in this study.

The rate of heat release by the condenser can be calculated as follows:

$$\dot{Q}_{COND} = \dot{m}_{wf}(h_8 - h_5) \quad (26)$$

Exergy analysis

Second law of thermodynamic or exergy analysis is a powerful tool to examine a thermodynamic system. The amount of energy efficiency loss, location, and cause can be found and specified reasonably with exergy analysis. In the exergy analysis method, each cycle component's irreversibility is obtained, and the irreversibility of the whole cycle can be calculated. The theory related to exergy analysis is presented in detail in references [22,23,44–48].

For an assumed control volume in steady state condition, the exergy conservation relation is presented as follows:

$$\dot{E}x_Q - \dot{E}x_W = \sum_e \dot{m}_e ex_e - \sum_i \dot{m}_i ex_i + \dot{E}x_D \quad (27)$$

Net exergy transferred by heat, as well as exergy resulting from the exchange of work, are expressed according to the following relations:

$$\dot{E}x_Q = \sum\left(1 - \frac{T_o}{T}\right)\dot{Q} \quad (28)$$

$$\dot{E}x_W = \dot{W} \quad (29)$$

In equation (27) the specific exergy relation, ex, can be expressed by the following:

$$ex = h - h_o - T_o(s - s_o) \quad (30)$$

The index *o* represents the dead state, which is considered equivalent to the ambient conditions, i.e., $T_o = 25\ ^\circ C$ and $P_o = 1$ atm [49].

In the ORC, the source of exergy is the fuel:

$$\dot{E}x_s = \dot{m}_f ex_f \quad (31)$$

The following equation calculates specific fuel exergy:

$$ex_f = \xi_f LHV \quad (32)$$

In the above relationship, LHV is the fuel's low heating value and ξ_f is the exergy factor of the fuel.

Exergy destruction occurs in various system components, including PEM FC, Air compressor, Fuel pressure regulating valve, HRVG, expander, condenser, and pump. For each equipment in the studied system, the rate of exergy destruction is calculated based on the expressions tabulated in Table 1.

Table 1 – Expressions for exergy destruction rate of the system's components.

Component	Exergy destruction rate expression
Air Compressor	$\dot{E}x_{D,COMP} = \dot{E}x_2 - \dot{E}x_3 + \dot{E}x_{W,COMP}$
Fuel pressure regulating valve	$\dot{E}x_{D,valve} = \dot{E}x_1 - \dot{E}x_{1a}$
PEM FC	$\dot{E}x_{D,FC} = \dot{E}x_{1a} + \dot{E}x_3 - \dot{E}x_{W,FC} - \dot{E}x_{1b} - \dot{E}x_4$
HRVG	$\dot{E}x_{D,HRVG} = \sum \dot{E}x_{in,HRVG} - \sum \dot{E}x_{out,HRVG}$
Expander	$\dot{E}x_{D,EXP} = \dot{E}x_7 - \dot{E}x_8 - \dot{E}x_{W,EXP}$
Condenser	$\dot{E}x_{D,COND} = \sum \dot{E}x_{in,COND} - \sum \dot{E}x_{out,COND}$
Pump	$\dot{E}x_{D,PMP} = \dot{E}x_5 + \dot{E}x_{W,PMP} - \dot{E}x_6$

Exergy efficiency is the ratio of actual heat efficiency to maximum reversible heat efficiency under similar conditions. In general, the exergy efficiency is defined as follows:

$$\eta_{ex} = 1 - \frac{Exergy\ destroyed}{Exergy\ supplied} \quad (33)$$

Economic analysis

In this study, the economic analysis is done by considering each system equipment's total cost rate (TCR). To this end, relations for estimating the purchase cost of each system component are presented first. These relationships are shown in Table 2.

The TCR of each system component in $/h is defined as:

$$\dot{Z} = \frac{Z\ CRF\ \Phi}{\tau N} \quad (34)$$

In the above relationship, Φ, N, and τ are the maintenance factor, nominal operating life, and annual operating hours, which are considered 5% and 20 years, and 7000 h, respectively [28,50]. Also, CRF represents the total operating period, which is calculated using the following equation [29,30]:

Table 2 – Purchase equipment cost of the system's component [24–27,31].

Component	Purchase equipment cost expression ($)
Air Compressor	$Z_{COMP} = 71.1\left(\frac{\dot{m}_{air}}{0.95 - \eta_{comp}}\right)\left(\frac{P_{FC}}{P_{amb}}\right)\log\left(\frac{P_{FC}}{P_{amb}}\right)$
PEM FC	$Z_{FC} = 1219.7\left(\frac{\dot{W}_{FC}}{1000}\right)$
Electricity inverter	$Z_{INV} = 10^5\left(\frac{\dot{W}_{FC}}{500000}\right)^{0.7}$
HRVG	$Z_{HRVG} = 276(A_{HRVG})^{0.88}$
Expander	$Z_{EXP} = 4750(\dot{W}_{EXP})^{0.75} + 60(\dot{W}_{EXP})^{0.95}$
Condenser	$Z_{COND} = 150(A_{COND})^{0.80}$
Pump	$Z_{PMP} = 3500(\dot{W}_{PMP})^{0.41}$
CRT	$Z_{CRT} = (31.5 + 16V_{CRT})/0.98$
Electricity generator	$Z_{GEN} = 60(G_{GEN})^{0.95}$
Instrument and control system	$Z_{INS} = 510$

$$CRF = i_{eff}\frac{(1+i)^n}{(1+i)^n-1} \quad (35)$$

In the above relationship, i represents the interest rate, and n represents the total operating period of the system in years. The TCR of the studied system can be calculated from the sum of the cost rates of individual components as follows:

$$TCR = \sum \dot{Z}_i \quad (36)$$

Exergoenvironmental analysis

Based on the exergy destruction rate, the exergoenvironmental assessment examines system performance from an environmental standpoint. An increase in exergy demolition rates negatively affects the performance of a system. It is due to this issue that there is a greater amount of fuel being used, which can have a detrimental effect on the environment as a result [51].

The term 'EEI' is used here to describe the exergoenvironmental index, which has the following definition:

$$EEI = \frac{total\ exergy\ destrcution\ rate}{total\ input\ exergy\ rate} \quad (37)$$

In order to calculate the environmental damage effectiveness index (EDEI), the following formula is used:

$$EDEI = \frac{EEI}{\eta_{ex}} \quad (38)$$

A definition of the exergy stability factor (ESF) can be found below:

$$ESF = \frac{total\ exergy\ destrcution\ rate}{total\ exergy\ destrcution\ rate + net\ electricity + 1} \quad (39)$$

Results and discussion

In this research, the optimal design of a PEM FC is discussed to maximize the exergy efficiency and minimize the TCR. Also, since the FC's electrochemical process is associated with heat release, an ORC using different zeotropic mixtures has been used as the cycle working fluid. The design variables include FC working temperature and pressure, FC current density, area of each FC, the number of FCs, PPTD of HRVG and condenser, and the mass fraction of working fluids in the zeotropic mixture.

Table 3 presents the parameters related to the study. At first, a parametric study was conducted, and the effect of different variables on the objective functions was investigated. Then, by performing a two-objective optimization, the optimal performance conditions of this combined power generation system are checked. It is necessary to explain since FCs undergo degradation over time. Also, to consider this factor in the overall cost rate of the system, it is assumed that the FC should be replaced every five years during the twenty-year life of the system (see Table 4).

Parametric study

Fig. 2-a shows the effect of FC operating pressure on exergy efficiency and TCR for different zeotropic mixtures. As shown, with increasing pressure, exergy efficiency first increases, reaches the maximum value, and then decreases. Changes in exergy efficiency can be justified by the behavior of FC output power based on FC operating pressure. As can be seen, with increasing pressure, the net output power of the FC increases at first and decreases after reaching the maximum value. As seen in Fig. 2-b, due to the increased working pressure of the FC, the penetration of reactive gases increases and causes a decrease in the transport resistance, which leads to an increase in the output power. However, it should also be noted that high working pressure requires more air compression power. As a result, the work of the compressor increases, which ultimately leads to a decrease in the FC net output power.

Fig. 3-a shows the effect of FC operating temperature on exergy efficiency and TCR. As can be seen, the increase in temperature leads to both exergy efficiency and TCR rises, receiving their maximum value and then decreasing slightly. Also, Fig. 3b illustrates the net output power of the ORC and PEM FC by increasing the FC operating temperature. As shown by increasing the FC operating temperature, its net output power increases, and decreases. This is because by increasing the operating temperature, the chemical reaction of the FC takes place faster since the membrane resistance decreases. Then by more operating temperature, the losses increase, leading to FC net output power decrement. On the other hand, the increase in temperature leads to a rise in the heat generated by the FC and an increase in the power production of the ORC system. As can be seen, the rise in temperature results in addition in

Table 3 – Parameters of the considered system.

n_e	Number of electrons	2
F	Faraday constant	96.485 $\frac{C}{mol}$
R	Universal gas constant	8.314 $\frac{J}{mol.K}$
T_{amb}	Ambient temperature	293.15 K
P_{amb}	Ambient pressure	101.325 kPa
i_L	Limiting current density	1.5 $\frac{A}{cm^2}$
L	Membrane thickness	0.00254 cm
λ_{air}	Stoichiometric rate of air	2
λ_{H_2}	Stoichiometric rate of hydrogen	1.2
HHV	Higher heating value of hydrogen	285.55 $\frac{kJ}{mol}$

Table 4 – Decision variables and considered range for the study.

Decision Variables	Value in parametric study	Range
Pressure of FC (kPa)	250	[101, 501]
Temperature of FC (K)	360	[350,373]
Current Density (A/cm^2)	0.10	[0.01,1.5]
FC Area (cm^2)	220	[150,300]
FC Quantity (–)	5000	[500,10,000]
PPTD of HRVG (°C)	10	[5,15]
PPTD of Condenser (°C)	10	[5,15]
Zeotropic mixture Fraction (–)	0.5	[0,1]

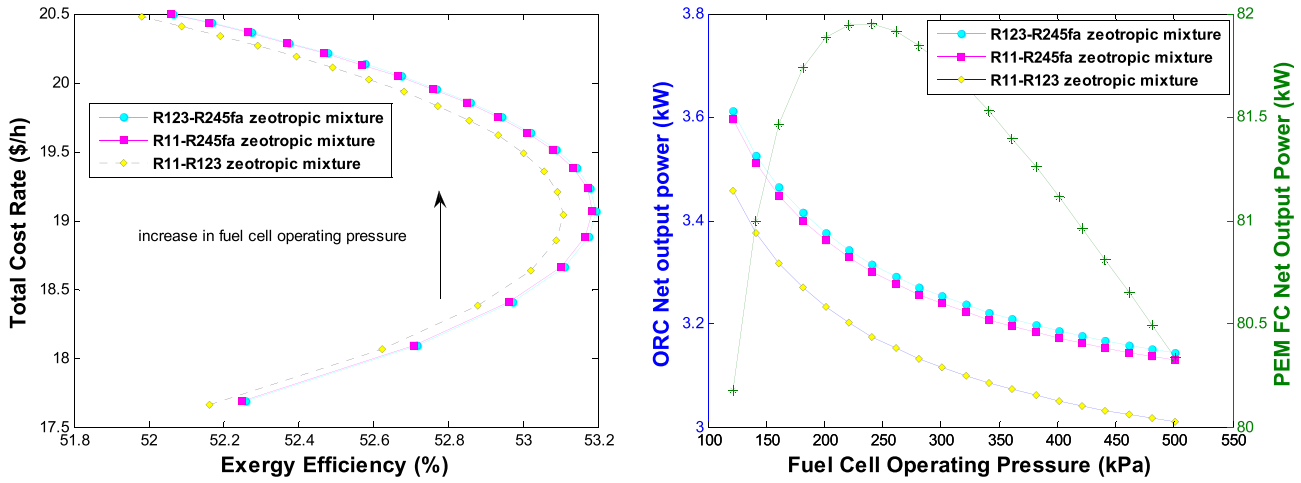

Fig. 2 – Effect of PEM FC operating pressure in Exergy efficiency and total cost rate (left: 2a) effect of PEM FC operating pressure in ORC and PEMFC net output power (right: 2b).

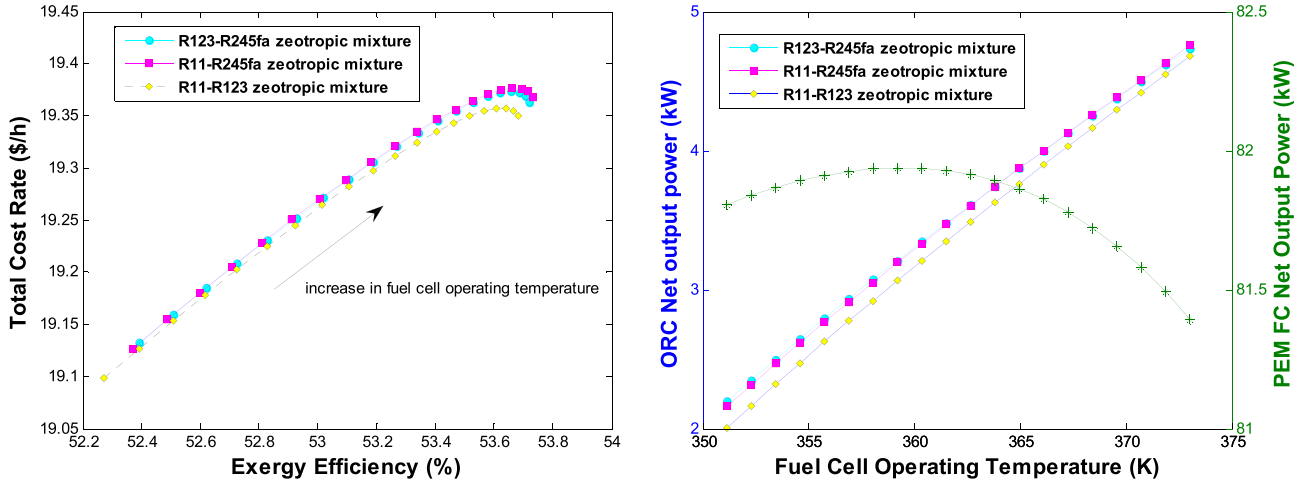

Fig. 3 – Effect of PEM FC operating temperature in Exergy efficiency and total cost rate (left: 3a) effect of PEM FC operating temperature in ORC and PEMFC net output power (right: 3b).

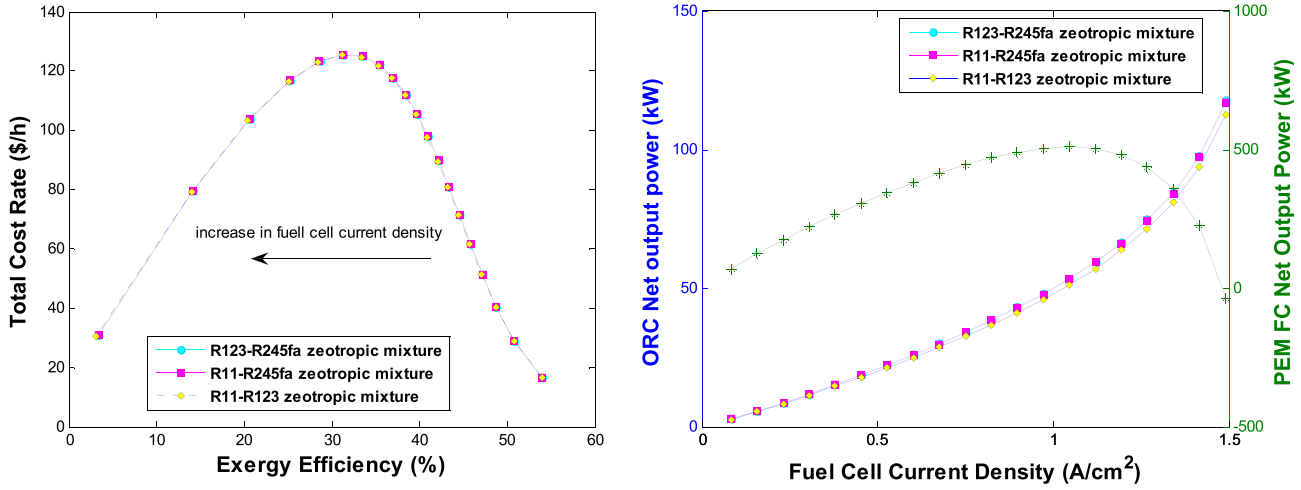

Fig. 4 – Effect of PEM FC current density in Exergy efficiency and total cost rate (left: 4a) effect of PEM FC current density in ORC and PEMFC net output power (right: 4b).

the TCR, although the rate of increase in both objective functions is almost the same.

Fig. 4a shows the effect of increasing current density on exergy efficiency and the TCR of the system. As can be seen, the increase in current density has a significant impact in exergy efficiency. It continuously decreases exergy efficiency because it leads to an increase in free electrons and an increase in irreversibilities. Fig. 4b provides the effect of current density on the ORC and PEM FC net output power. As current density increases, PEM FC power increases and then decreases. So, there is an optimum value for the current density from net power and exergy efficiency points of view. Increasing the current density, the FC heat generation increases, and the ORC power increases, too. Regarding the TCR of the system, increasing the current density first causes an increase and then a decrease. This is mainly due to the variation of the PEM FC power with current density.

Fig. 5a depicts the effect of increasing the FC area on the objective functions of the system. As can be seen, increasing the cross-sectional area causes a significant increase in the TCR while not significantly improving exergy efficiency. Also, by increasing the PEM FC area, its net output power increases linearly. Also, the ORC net output power increases due to increases in PEM FC heat generation.

Fig. 6a shows the effect of increasing the number of FCs on the objective functions. As can be seen, the increase in the number of FCs does not affect the exergy efficiency because the rise in fuel consumption and the increase in production power increase proportionally while the TCR is increasing. As predicted and depicted in Fig. 6b, increasing the number of FCs, the output power of both FC and ORC increases linearly.

Fig. 7a shows the impact of PPTD of HRVG on exergy efficiency and TCR of the system. As can be seen, decreasing the PPTD of HRVG leads to an increase in the exergy efficiency and a slight increase in the TCR. Also, Fig. 7b illustrates the net output power of the ORC by increasing the HRVG PPTD. By increasing this design parameter, ORC net output power decreases. This is due to lower heat recovery from the FC.

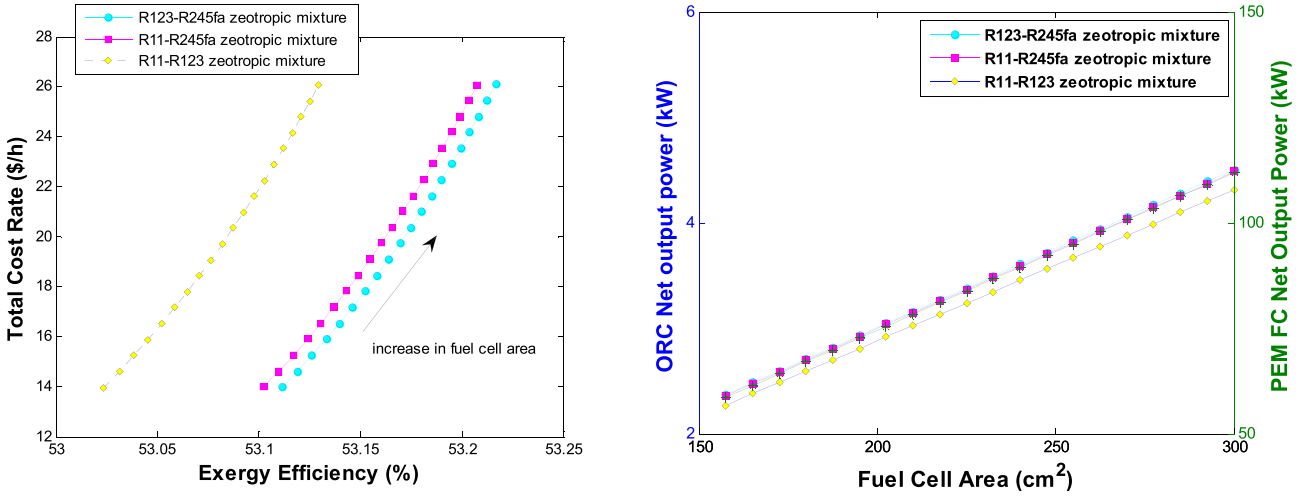

Fig. 5 – Effect of PEM FC area in Exergy efficiency and total cost rate (left: 5a) effect of PEM FC are in ORC and PEMFC net output power (right: 5b).

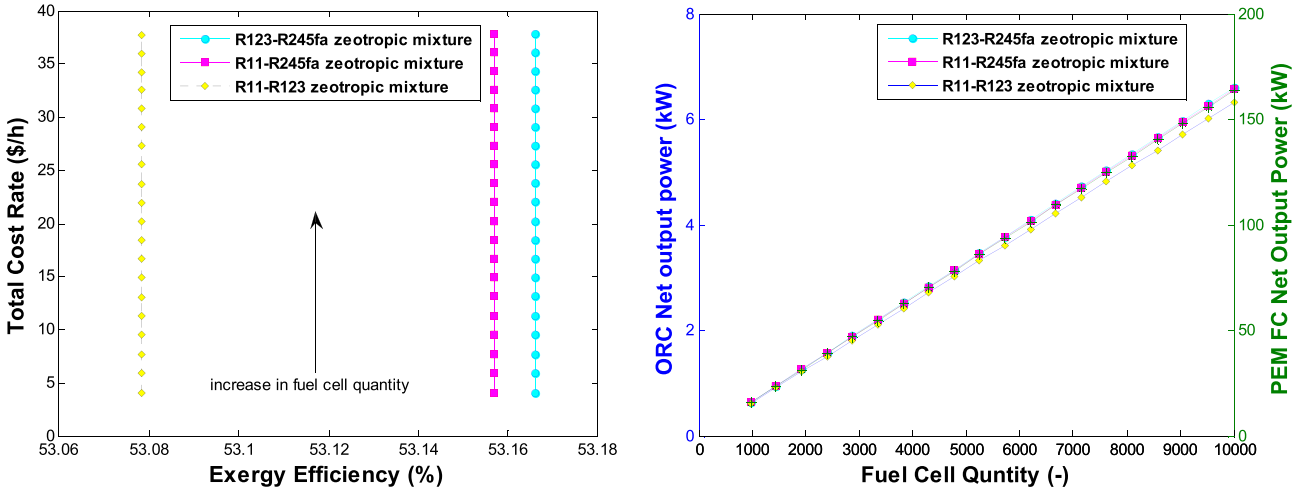

Fig. 6 – Effect of PEM FC quantity in Exergy efficiency and total cost rate (left: 6a) effect of PEM FC quantity in ORC and PEMFC net output power (right: 6b).

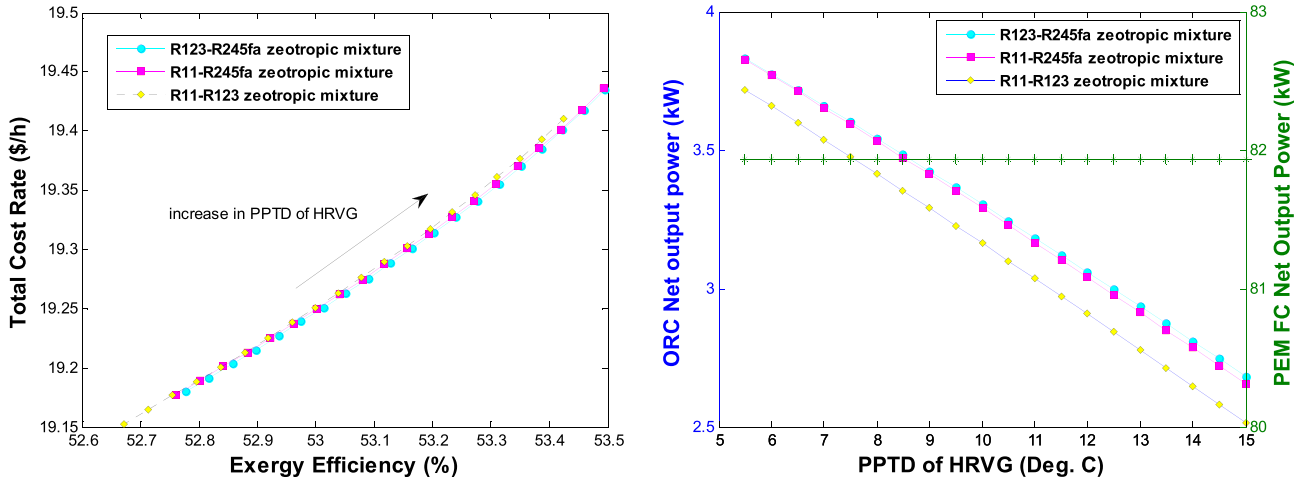

Fig. 7 – Effect of PPTD of HRVG in Exergy efficiency and total cost rate (left: 7a) effect of PPTD of HRVG in ORC and PEMFC net output power (right: 7b).

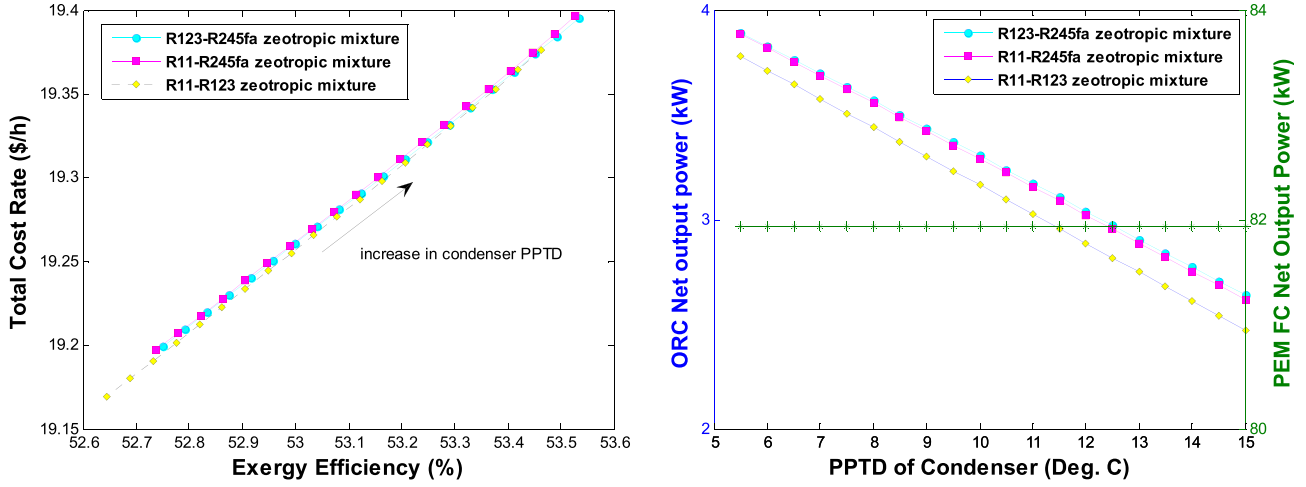

Fig. 8 – Effect of PPTD of the condenser in Exergy efficiency and total cost rate (left: 8a) effect of PPTD of the condenser in ORC and PEMFC net output power (right: 8b).

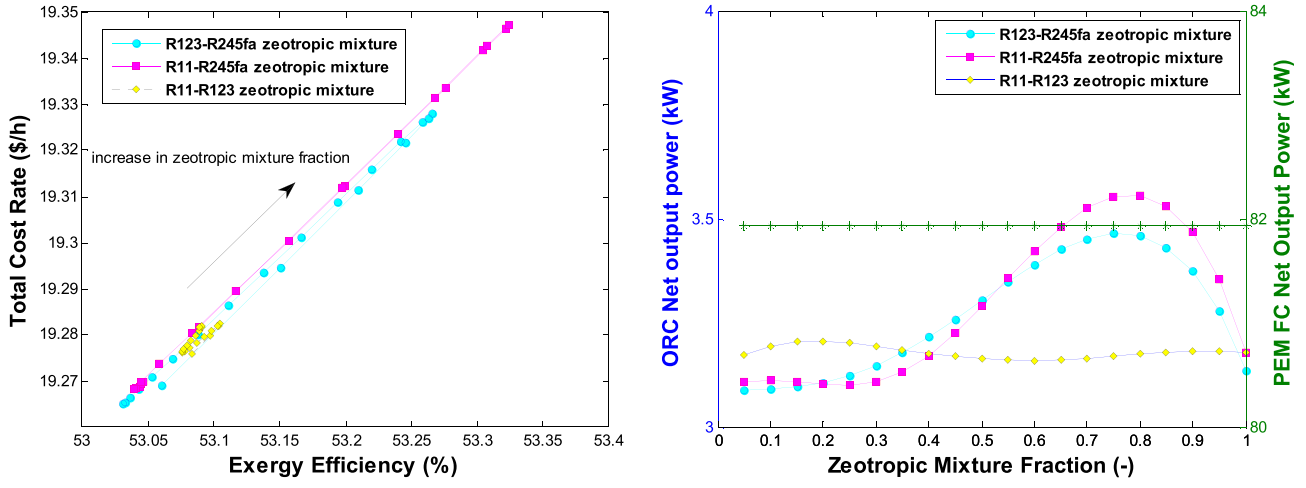

Fig. 9 – Effect of zeotropic mixture fraction in Exergy efficiency and total cost rate (left: 9a) effect of zeotropic mixture fraction in ORC and PEMFC net output power (right: 9b).

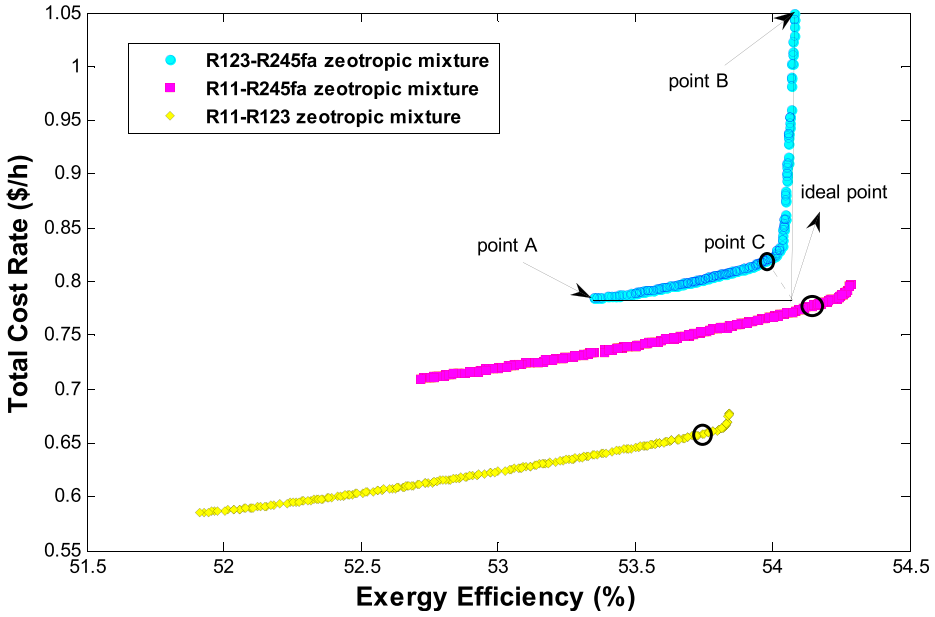

Fig. 10 – Pareto fronts of the present study.

Fig. 8a depicts the effect of condenser PPTD on the objective functions of the study. Just like the HRVG PPTD, increasing the condenser PPTD increases both exergy efficiency and TCR. Also, as shown in Fig. 8b, the net output power of the ORC decreases by increasing the condenser PPTD.

Fig. 9a illustrates the effect of zeotropic mixture fraction on the exergy efficiency and TCR of the system. as shown, there is an optimum value for the mixture fraction. Fig. 9b shows the effect of the zeotropic mixture fraction on ORC net output power. As shown, in the zeotropic mixture of R-11-R123, the working fluids' fraction does not have a considerable effect on the net output power. In contrast, for two other considered mixtures, the optimum value of the ORC net output power can be reached by increasing the mixture fraction to about 0.75.

Fig. 10 illustrates the Pareto front related to the present study for three different zeotropic fluids. In this study, two objective functions of exergy efficiency and TCR are considered for the optimization process. To this end, an evolutionary genetic algorithm is used for optimization. Since these two objective functions are in contrast with each other and optimizing one alone causes the other objective function to move away from the optimal state, it is necessary to draw the Pareto front and select the final optimal point based on technical and economic priorities among the front points. He chose the Pareto. In the Pareto front, each point is an optimal design with a different approach from the rest of the points. Point A in Fig. 10 is an optimal point considering only the overall cost rate as the objective function. Therefore, TCR is at its minimum value. In this situation, the optimality of exergy efficiency has not been considered. Also, point C is an optimal point considering only exergy efficiency as the objective function and the maximum possible value of exergy efficiency has been achieved. In this case, no attention has been paid to TCR optimization. The best design is when the exergy efficiency has its maximum possible value (i.e. point C) and the TCR has its minimum possible value (i.e. point A). This point is called ideal point. Which, of course, is not the point of the Pareto front, and it is practically impossible to reach this point. Therefore, the closest point to this point can be considered as an optimal design. This point is marked in the figure for each of the zeotropic fluids and their performance information is presented in Table 5. As can be seen, the optimal point related to the zeotropic mixture R11-R245fa has the highest exergy efficiency and the optimal point related to the zeotropic mixture R11-R123 has the lowest TCR. Choosing the final optimal design point can be chosen according to different considerations, including technical, economic and operational considerations. In terms of environment, the exergoenvironmental index, environmental damage

Table 5 – Operating parameters of the selected optimal design points.

Working fluid	R123-R245fa	R11-R245fa	R11-R123
Exergy Efficiency (%)	53.99	54.15	53.75
Total cost rate ($/h)	0.82	0.77	0.65
Pressure of FC (kPa)	227.0	208.2	129.80
Exergoenvironmental index (-)	0.5105	0.5230	0.4750
Environmental damage effectiveness index (-)	1.361	1.297	1.277
Exergy stability factor (-)	0.5676	0.5576	0.5506
Temperature of FC (K)	369.4	364.5	351.50
Current Density (A/cm^2)	0.1	0.1	0.10
FC Area (cm^2)	170.60	158.35	150.05
FC Quantity (–)	530	562	501
PPTD of HRVG (°C)	5.11	5.74	5.50
PPTD of Condenser (°C)	5.05	5.48	9.0
Zeotropic mixture Fraction (–)	0.14	0.27	0.92

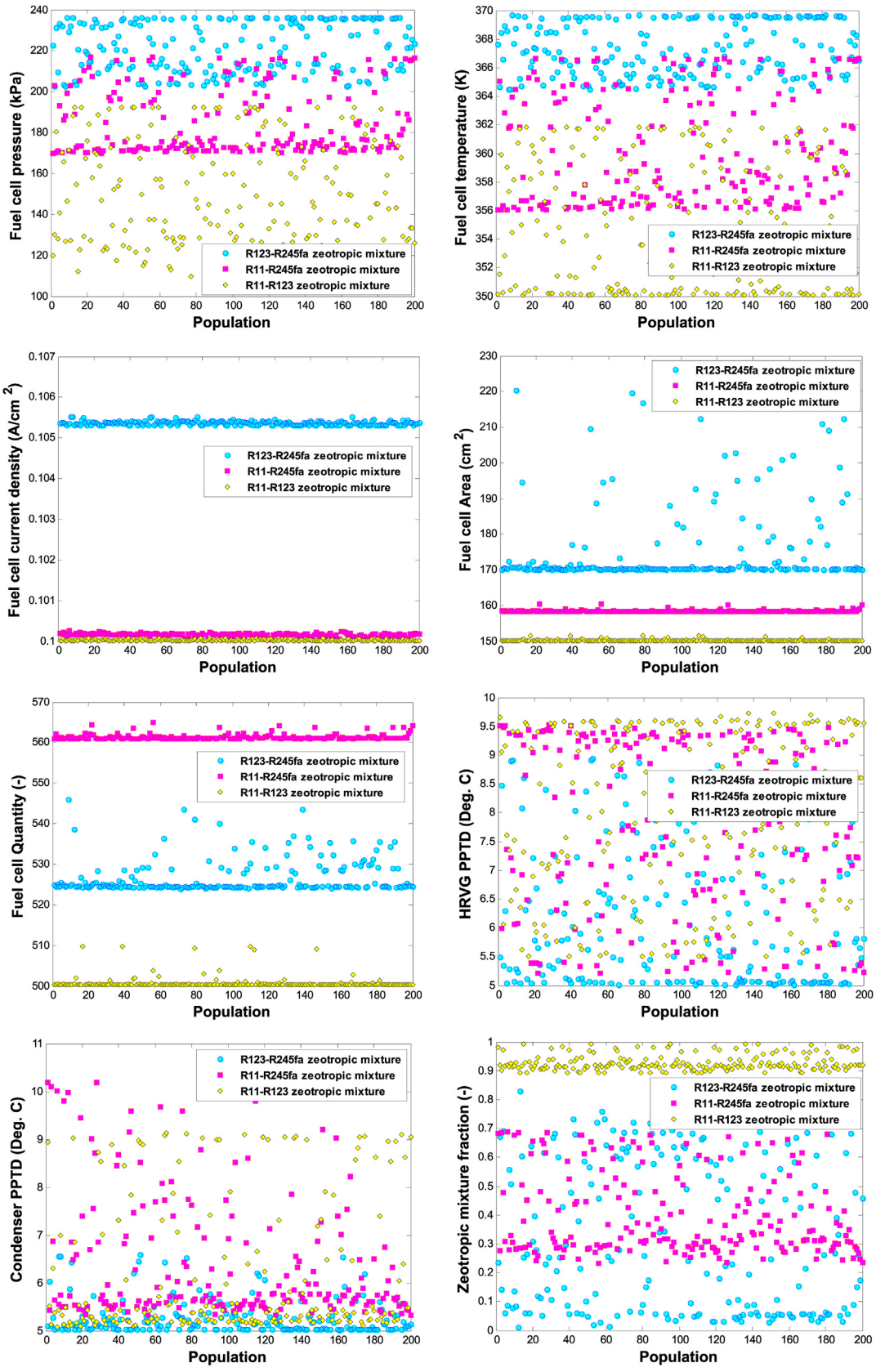

Fig. 11 – Design variables scattering point belongs to the Pareto fronts.

effectiveness index, and exergy stability factor of the zeotropic mixture R11-R123 are 0.5506, 1.277, and 0.4750, respectively.

Fig. 11 shows the scattering of design variables for different zeotropic mixtures and points of the Pareto front.

Conclusion

In this study, the multi-objective optimization design of a hybrid power generation system is discussed. This system includes a PEM FC and an ORC system using different zeotropic mixtures as working fluids. PEM FC design variables include operating pressure and temperature, current density, FC cross-section, and number of FCs, and ORC system design variables include PPTD of HRVG, PPTD of Condenser, and zeotropic mixture ratio. A parametric analysis was performed to investigate the effect of design variables. Finally, the system design was done for three different zeotropic mixtures, including R11-R123, R11-R245fa, and R123-R245fa.

It is observed applying zeotropic mixtures improves the exergy efficiency of the ORC system by decreasing the exergy destruction in the HRVG. Also, it is shown operating pressure and temperature of FC have an optimum value from exergy efficiency and power production points of view. While the increase in FC area leads to a significant increase in power production and also a slight increase in the exergy efficiency of the system. Also, it is observed the increase in current density has an optimal value from the point of view of power production and exergy efficiency of the system. The optimal design point with the highest exergy efficiency is observed for R11-R245fa with a value of 54.15% and the optimal design point with the lowest TCR It is related to the zeotropic mixture R11-R123 with a value of 0.65 $/s. Environmentally, the exergoenvironmental index, environmental damage effectiveness index, and exergy stability factor for the zeotropic mixture R11-R123 are equal to 0.5506, 1.277, and 0.4750, respectively, which is the best zeotropic mixture in comparison with others.

Declaration of competing interest

The authors declare that they have no known competing financial interests or personal relationships that could have appeared to influence the work reported in this paper.

Acknowledgements

A. This research was funded by Key Laboratory of Advanced Manufacturing Technology of the Ministry of Education of Guizhou University (GZUAMT2022KF[07]); the National Natural Science Foundation of China under Grant No(61862051); the Science and Technology Foundation of Guizhou Province under Grant No.(ZK[2022]549); the Natural Science Foundation of Education of Guizhou province under Grant No.[2019]203; the program of Qiannan Normal University for Nationalities under Grant No.(qnsy2018003, qnsy2019rc09).

B. This study is supported via funding from Prince sattam bin Abdulaziz University project number (PSAU/2023/R/1444).

C. Researchers Supporting Project number (RSP-2023/303), King Saud University, Riyadh, Saudi Arabia.

REFERENCES

[1] Cengel Yunus A, Boles Michael A, Kanoğlu Mehmet. Thermodynamics: an engineering approach, vol. 5. New York: McGraw-hill; 2011.

[2] Musharavati F, Khoshnevisan A, Alirahmi SM, Ahmadi P, Khanmohammadi S. Multi-objective optimization of a biomass gasification to generate electricity and desalinated water using Grey Wolf Optimizer and artificial neural network. Chemosphere 2022;287:131980.

[3] Briguglio N, Ferraro M, Brunaccini G, Antonucci V. Evaluation of a low temperature fuel cell system for residential CHP. Int J Hydrogen Energy 2011;36(13):8023–9.

[4] Aki H, Yamamoto S, Ishikawa Y, Kondoh J, Maeda T, Yamaguchi H, Ishii I. Operational strategies of networked fuel cells in residential homes. IEEE Trans Power Syst 2006;21(3):1405–14.

[5] Nguyen HQ, Shabani B. Proton exchange membrane fuel cells heat recovery opportunities for combined heating/cooling and power applications. Energy Convers Manag 2020;204:112328.

[6] Placca L, Kouta R, Candusso D, Blachot JF, Charon W. Analysis of PEM fuel cell experimental data using principal component analysis and multi linear regression. Int J Hydrogen Energy 2010;35(10):4582–91.

[7] Sevjidsuren G, Uyanga E, Bumaa B, Temujin E, Altantsog P, Sangaa D. Exergy analysis of 1.2 kW NexaTM fuel cell module. In: Clean energy for better environment. IntechOpen; 2012.

[8] Grujicic M, Chittajallu KM. Design and optimization of polymer electrolyte membrane (PEM) fuel cells. Appl Surf Sci 2004;227(1–4):56–72.

[9] Kazim A. Exergy analysis of a PEM fuel cell at variable operating conditions. Energy Convers Manag 2004;45(11–12):1949–61.

[10] Salva JA, Iranzo A, Rosa F, Tapia E, Lopez E, Isorna F. Optimization of a PEM fuel cell operating conditions: obtaining the maximum performance polarization curve. Int J Hydrogen Energy 2016;41(43):19713–23.

[11] Hwang JJ, Zou ML, Chang WR, Su A, Weng FB, Wu W. Implementation of a heat recovery unit in a proton exchange membrane fuel cell system. Int J Hydrogen Energy 2010;35(16):8644–53.

[12] Azad A, Fakhari I, Ahmadi P, Javani N. Analysis and optimization of a fuel cell integrated with series two-stage organic Rankine cycle with zeotropic mixtures. Int J Hydrogen Energy 2022;47(5):3449–72.

[13] Li Z, Khanmohammadi S, Khanmohammadi S, Al-Rashed AA, Ahmadi P, Afrand M. 3-E analysis and optimization of an organic rankine flash cycle integrated with a PEM fuel cell and geothermal energy. Int J Hydrogen Energy 2020;45(3):2168–85.

[14] Li YZ. Thermodynamic analysis of polymer-electrolyte-membrane fuel-cell performance under varying cooling conditions. Int J Hydrogen Energy 2012;37(14):10798–806.

[15] Ye L, Jiao K, Du Q, Yin Y. Exergy analysis of high-temperature proton exchange membrane fuel cell systems. Int J Green Energy 2015;12(9):917–29.

[16] Gimba ID, Abdulkareem AS, Jimoh A, Afolabi AS. Theoretical energy and exergy analyses of proton exchange membrane

fuel cell by computer simulation. J Appl Chem 2016;2016:1–15.
[17] Barelli L, Bidini G, Gallorini F, Ottaviano A. An energetic–exergetic analysis of a residential CHP system based on PEM fuel cell. Appl Energy 2011;88(12):4334–42.
[18] Lupanov VP. Nitraty pri ishemicheskoy bolezni serdtsa v zavisimosti ot klinicheskoy formy i tyazhesti zabolevaniya. Consilium Medicum 2006;8(5):91–9.
[19] Kim HI, Cho CY, Nam JH, Shin D, Chung TY. A simple dynamic model for polymer electrolyte membrane fuel cell (PEMFC) power modules: parameter estimation and model prediction. Int J Hydrogen Energy 2010;35(8):3656–63.
[20] Wu J, Yuan XZ, Wang H, Blanco M, Martin JJ, Zhang J. Diagnostic tools in PEM fuel cell research: Part I Electrochemical techniques. Int J Hydrogen Energy 2008;33(6):1735–46.
[21] Tahani M, Javan S, Biglari M. A comprehensive study on waste heat recovery from internal combustion engines using organic Rankine cycle. Therm Sci 2013;17(2):611–24.
[22] Rosen MA, Dincer I. A study of industrial steam process heating through exergy analysis. Int J Energy Res 2004;28(10):917–30.
[23] Seyedkavoosi Seyedali, Javan Saeed, Krishna Kota. Exergy-based optimization of an organic Rankine cycle (ORC) for waste heat recovery from an internal combustion engine (ICE). Appl Therm Eng 2017;126:447–57.
[24] Bejan A, Tsatsaronis G, Moran MJ. Thermal design and optimization. John Wiley & Sons; 1995.
[25] Peters MS, Timmerhaus KD, West RE. Plant design and economics for chemical engineers, vol. 4. New York: McGraw-hill; 2003.
[26] Quoilin S, Declaye S, Tchanche BF, Lemort V. Thermo-economic optimization of waste heat recovery Organic Rankine Cycles. Appl Therm Eng 2011;31(14–15):2885–93.
[27] Dincer I, Rosen MA, Ahmadi P. Optimization of energy systems. John Wiley & Sons; 2017.
[28] Fakhari I, Behzadi A, Gholamian E, Ahmadi P, Arabkoohsar A. Comparative double and integer optimization of low-grade heat recovery from PEM fuel cells employing an organic Rankine cycle with zeotropic mixtures. Energy Convers Manag 2021;228:113695.
[29] Gholamian E, Zare V, Javani N, Ranjbar F. Dynamic 4E (energy, exergy, economic and environmental) analysis and tri-criteria optimization of a building-integrated plant with latent heat thermal energy storage. Energy Convers Manag 2022;267:115868.
[30] Burulday ME, Mert MS, Javani N. Thermodynamic analysis of a parabolic trough solar power plant integrated with a biomass-based hydrogen production system. Int J Hydrogen Energy 2022;47(45):19481–501.
[31] Bo Z, Mihardjo LW, Dahari M, Abo-Khalil AG, Al-Qawasmi A, Mohamed AM, et al. Thermodynamic and exergoeconomic analyses and optimization of an auxiliary tri-generation system for a ship utilizing exhaust gases from its engine. J Cleaner Production 2021;287:125012. https://doi.org/10.1016/j.jclepro.2020.125012.
[32] Anqi AE, Li C, Dhahad HA, Sharma K, Attia E-A, Abdelrahman A, et al. Effect of combined air cooling and nano enhanced phase change materials on thermal management of lithium-ion batteries. J Energy Storage 2022;52:104906. https://doi.org/10.1016/j.est.2022.104906.
[33] Li L, Zhang D, Deng J, Gou Y, Fang J, …, Cui H, et al. Carbon-based materials for fast charging lithium-ion batteries. Carbon 2021;183:721–34. https://doi.org/10.1016/j.carbon.2021.07.053.
[34] Wang C, Sheng L, Jiang M, Lin X, Wang Q, Guo M, et al. Flexible SnSe2/N-doped porous carbon-fiber film as anode for high-energy-density and stable sodium-ion batteries. J Power Sources 2023;555:232405. https://doi.org/10.1016/j.jpowsour.2022.232405.
[35] Li R, Du Z, Qian X, Li Y, Martinez-Camarillo JC, Jiang L, et al. High resolution optical coherence elastography of retina under prosthetic electrode. Quant Imaging Med Surg 2021 Mar;11(3):918–27. https://doi.org/10.21037/qims-20-1137.
[36] Sharma P, Said Z, Kumar A, et al. Recent advances in machine learning research for nanofluid-based heat transfer in renewable energy system. Energy & Fuels 2022;36(13):6626–58. https://doi.org/10.1021/acs.energyfuels.2c01006.
[37] Yang YY, Gong YD, Li CH, Wen XL, Sun JY. Mechanical performance of 316L stainless steel by hybrid directed energy deposition and thermal milling process. J Mater Processing Technol 2021;291:117023. https://doi.org/10.1016/j.jmatprotec.2020.117023.
[38] Hassan F, Jamil F, Hussain A, Ali GM, Janjua MM, Khushnood S, et al. Recent advancements in latent heat phase change materials and their applications for thermal energy storage and buildings: A state of the art review. Sustain Energy Technol Assessments 2022;49:101646. https://doi.org/10.1016/j.seta.2021.101646.
[39] Ejaz A, Babar H, Ali HM, Jamil F, Janjua MM, Fattah IR, et al. Concentrated photovoltaics as light harvesters: Outlook, recent progress, and challenges. Sustain Energy Technol Assess 2021;46:101199. https://doi.org/10.1016/j.seta.2021.101199.
[40] Cao Y, Dhahad HA, Hussen HM, Anqi AE, Farouk N, Parikhani T. Multi-objective optimization of a dual energy-driven solid oxide fuel cell-based power plant. Appl Thermal Eng 2021;198:117434. https://doi.org/10.1016/j.applthermaleng.2021.117434.
[41] Cai K, Wang T, Wang Z, Wang J, Li L, …, Yao C, et al. A cocklebur-like sulfur host with the TiO2-VOx heterostructure efficiently implementing one-step adsorption-diffusion-conversion towards long-life Li–S batteries. Composites Part B: Engineering 2023;249:110410. https://doi.org/10.1016/j.compositesb.2022.110410.
[42] Zhang D, Tan C, Ou T, Zhang S, Li L, …, Ji X. Constructing advanced electrode materials for low-temperature lithium-ion batteries: A review. Energy Reports 2022;8:4525–34. https://doi.org/10.1016/j.egyr.2022.03.130.
[43] Cao Y, Dhahad HA, Togun H, Hussen HM, Anqi AE, Farouk N, et al. Effect of working fluids in a novel geothermal-based integration of organic-flash and power/cooling generation cycles with hydrogen and freshwater production units. International Journal of Hydrogen Energy 2021;46(56):28370–86. https://doi.org/10.1016/j.ijhydene.2021.06.129.
[44] Yang C, Guo R, Jing X, Li P, Yuan J, …, Wu Y. Degradation mechanism and modeling study on reversible solid oxide cell in dual-mode — A review. Int J Hydrogen Energy 2022;47(89):37895–928. https://doi.org/10.1016/j.ijhydene.2022.08.240.
[45] Lu S, Yin Z, Liao S, Yang B, Liu S, Liu M, et al. An asymmetric encoder–decoder model for Zn-ion battery lifetime prediction. Energy Reports 2022;8:33–50. https://doi.org/10.1016/j.egyr.2022.09.211.
[46] Cao Y, Mihardjo LW, Dahari M, Mustafa Mohamed A, Ghaebi H, Parikhani T. Assessment of a novel system utilizing gases exhausted from a ship's engine for power, cooling, and desalinated water generation. Appl Thermal Eng 2021;184:116177. https://doi.org/10.1016/j.applthermaleng.2020.116177.
[47] Cao Y, Mihardjo LW, Dahari M, Ghaebi H, Parikhani T, Mohamed AM. An innovative double-flash binary cogeneration cooling and power (CCP) system: Thermodynamic evaluation and multi-objective

optimization. Energy 2021;214:118864. https://doi.org/10.1016/j.energy.2020.118864.
[48] Bahman AM, Parikhani T, Ziviani D. Multi-objective optimization of a cold-climate two-stage economized heat pump for residential heating applications. J Building Eng 2022;46:103799. https://doi.org/10.1016/j.jobe.2021.103799.
[49] Cao Y, Dhahad HA, Hussen HM, Parikhani T. Proposal and evaluation of two innovative combined gas turbine and ejector refrigeration cycles fueled by biogas: Thermodynamic and optimization analysis. Renewable Energy 2022;181:749–64. https://doi.org/10.1016/j.renene.2021.09.043.
[50] Dhahad HA, Ahmadi S, Dahari M, Ghaebi H, Parikhani T. Energy, exergy, and exergoeconomic evaluation of a novel CCP system based on a solid oxide fuel cell integrated with absorption and ejector refrigeration cycles. Thermal Sci Eng Progress 2021;21:100755. https://doi.org/10.1016/j.tsep.2020.100755.
[51] Cao Y, Ehyaei MA. Energy, exergy, exergoenvironmental, and economic assessments of the multigeneration system powered by geothermal energy. J Clean Prod 2021;313:127823. https://doi.org/10.1016/j.jclepro.2021.127823.